Real Nuclear Fusion on a Tabletop

by John G. Cramer

Alternate View Column AV-139
Keywords: *nuclear, fusion, tabletop, deuterium, pyroelectric, crystal, neutron, energy, production*
Published in the October-2007 issue of ***Analog Science Fiction & Fact Magazine****;*

In the December-1989 issue of Analog, I wrote an AV Column entitled "Cold Fusion, Pro-fusion, and Con-fusion" that described and gave my opinions about the recently announced "discovery of cold fusion" by Stanley Pons and Martin Fleischmann. These University of Utah electro-chemists claimed that by electrolyzing D_2O (heavy water) on a tabletop, they had produced the nuclear fusion of deuterium (mass-2 hydrogen) nuclei inside a palladium electrode, generating lots of extra heat but no significant radiation. My column was written very early in that controversy and the dust had not completely settled, but it was clear to me at the time (and is still clear) that the reported results were an example of bad science and overblown claims.

By contrast, in this column I want to report on a well executed experiment performed by B. Naranjo, J. K. Gimzewski, and S. Putterman (NGP) of UCLA that demonstrates the ***successful*** production of the nuclear fusion of deuterium with a relatively simple tabletop experiment. It was reported in the April 28, 2005 issue of the science journal *Nature*. The announcement of this breakthrough produced hardly a blip in science-based news reports, perhaps because many science reporters had previously been burned by the overblown Pons and Fleischmann affair,.

So what is d+d nuclear fusion? Let's review the process. Nuclear fusion is the primary

energy source of the Sun. High temperatures and pressures near the Sun's center drive the fusion of hydrogen into helium, releasing lots of energy. Here on Earth, we would also like to use fusion as our primary energy source, but, with the exception of thermonuclear bomb explosions, we have yet to master the trick very well. One must bring two deuterium nuclei (mass-2 hydrogen containing a proton and a neutron) close enough together that they can fuse. This fusion could, in principle, form a single helium nucleus (2 protons + 2 neutrons), and a gamma ray, liberating about five million times more energy than could be obtained from any chemical reaction between two atoms.

However, there are several problems with achieving this. First, both deuteron nuclei have a positive electrical charge. When they get close, these charges repel, producing a large electrical force that pushes the nuclei apart. One must overcome this force with either high temperatures or acceleration to bring the deuterons close enough to fuse.

The second problem is that a fusion process must simultaneously obey the law of energy conservation and of momentum conservation. Because of this dual requirement, the d + d fusion reaction makes helium-3 plus a neutron or hydrogen-3 plus a proton with much higher probabilities than it makes helium-4 plus a gamma ray. Therefore, any d + d fusion reaction should be a prodigious source of fast neutrons, i.e., neutron radiation. As someone said in 1989, Stanley Pons' own announcement refuted his claims, because if his experiment had actually worked, he would have died of neutron exposure before reaching the microphone.

On the other hand, the NGP experiment ***does*** proceed by the d+d $\rightarrow$ ^{3}He+n reaction and ***does*** make lots of neutrons. It gets the deuterons close enough to fuse by accelerating one deuteron to a kinetic energy of about 115,000 electron-volts and slamming it into another at-rest deuterium atom by using a heated 1 cm thick ferroelectric crystal of $LiTaO_3$ (lithium tantalate) to produce a very large electric potential (~115,000 volts).

What?? A 1 cm thick crystal producing a 115 kilovolt electric potential??? That sounds like magic! Yes, I suppose it is magic in a way, the kind of quantum magic that occurs in some crystals and is called the ***ferroelectric process***.

To understand it, let's first consider ferromagnetism. The atoms of the metals iron, cobalt, and nickel contain little built-in magnetic compasses, each with its own little needle with a north and a south pole, called its magnetic dipole moment. Many materials have such magnetic moments, but in the ferromagnetic materials they like to line up to form a permanent magnet, with most of the atoms pointing their little compass needles in the same direction, so that a bar of the material has a definite north magnetic pole at one end, a south magnetic pole at the other end, and a fairly strong magnetic field around the bar. This occurs because, for subtle reasons involving quantum mechanics, a ferromagnetic system with the magnetic moments of its atoms lined up has a lower net energy than does one with the magnetic moments pointing in random directions. We have now seen this quantum magic in magnets so frequently that we take it for granted and use it to stick notes and pictures to our refrigerator doors without thinking about it.

A ferroelectric crystal works the much same way. Individual molecules of the crystal have an electric dipole moment, with a net positive electric charge on one end of the molecule and a negative charge on the other end. Again, for subtle reasons involving quantum mechanics, a ferroelectric crystal with its electric moments lined up has a lower energy than one with the electric moments pointing in random directions, creating a sheet of positive charge on one end of the crystal and a sheet of negative charge on the other. This is not a new discovery. It was first described by the Greek natural philosopher Theophrastus in 314 BC, it has been studied for many years by condensed-matter physicists and chemists, and it is already the basis for a commercial device that produces low-intensity X-rays.

In analogy with the poles of a permanent magnet, the ferroelectric crystal has a definite positive charge end and a negative charge end. Under the right circumstances, particularly when

it is heated (pyroelectricity), it develops a sizable electric potential between them. However, in air the electric field of a ferroelectric material is not so easy to observe because it is rapidly dissipated by polar molecules (e.g., water vapor) attracted to the surface and neutralizing the net charge. In a vacuum, however, this does not happen, and significant electric fields can be produced by the pyroelectric process as the crystal is heated.

The UCLA group placed a cylindrical 3 cm diameter by 1 cm thick ferroelectric lithium tantalate crystal in a vacuum vessel to which deuterium gas at a pressure of 0.7 Pa (0.0001 psi) had been admitted. The crystal was mounted with its negative end attached to a temperature-variable copper block and its positive end supporting a copper disc with a sharp tungsten spike at its center. The spike was 0.080 mm in diameter, 2.3 mm long, and had a tip radius of 100 nanometers. When the positive end of the crystal reached its maximum electric potential, the electric field near the tip of the tungsten spike was very large (greater than 25 volts per nanometer), strong enough to pull loose the electron from a deuterium atom and sent the positively charged nucleus in the other direction. Thus, a beam of ionized deuterium nuclei was given an energy of up to 115,000 electron-volts and directed against a grounded target plate placed opposite the crystal. The target plate supported a sheet of deuterated polyethylene, providing deuterium atoms with which the beam of deuteron ions could collide.

The crystal was temperature-cycled, first dropping its temperature to 240 K (-33 C) using liquid nitrogen and then progressively raising the temperature with electrical heating while observing the results with neutron and X-ray counters. After 100 seconds of heating, X-rays were observed from free electrons in the gas hitting the positive copper disc and crystal. After 160 seconds the neutron signal rose above background and increased rapidly until 220 seconds, when the heater was shut off. Neutron emission then began to drop as the deuteron beam bled off charge faster than the pyroelectric current could replace it, but strong neutron emission continued until 393 s when a spark discharged the system.

The reported measurements show clear evidence that the nuclear reaction d+d $\rightarrow {}^{3}$He+n had been produced, that the system had produced a deuteron beam ion current of 5 4.2 nA and had produced about 900 neutrons per second. Subsequent measurements at Rensselear Polytechnic Institute have confirmed the UCLA measurements. Therefore, a tabletop experiment has successfully produced controlled d+d fusion. This was accomplished using well established physical phenomena and has required no "visits from the Tooth Fairy" to make the process work.

There are some obvious improvements that could be made to the fusion demonstration configuration used by the UCLA group. First, there is no reason to attach only one sharp spike to the copper disc. As long as spikes on the disc are separated by distances greater than their length, they can operate as independent sources of deuterium ionization. Thus, one can imagine a "bed of nails" configuration using a copper disk equipped with perhaps 100 such tungsten spikes. This would in principle increase the fusion reaction rate and neutron yield by two orders of magnitude. Second, The Rensselear group has demonstrated that by using ***two*** pyroelectric crystals mounted in opposing positions with oppositely charging faces, the electric field can be doubled. For example, in the NGP configuration the deuterated target could be located on the negative face of a second pyroelectric crystal, with both crystals cooled and heated together, to produce a deuteron beam with a kinetic energy of 230 keV for the reactions, allowing the deuterons to travel further into the target and make more fusion reactions before losing too much energy to react. One could even think of stacking many crystals to achieve significantly larger potential differences. Third, if the target was made of a material loaded with tritium (mass-3 hydrogen) instead of deuterium (mass-2 hydrogen), the fusion reaction rate and neutron production rate would be about 100 times larger, and would produce neutrons that are 6 times more energetic (about 15 MeV instead of 2.5 MeV). We also note that by replacing the low pressure deuterium in the vacuum vessel with low-pressure helium-3, one could produce "radiation-free" energy with the d+^{3}He$\rightarrow {}^{4}$He+p fusion reaction, which produces no neutrons and

would be very easy to shield in a power-production context.

Thus, tabletop controlled fusion is now a reality! What does that mean? Are we on the brink of the new controlled fusion age of pollution-less and virtually free energy? Should we hold off buying a new car until the fusion-powered models become available? Sorry, it's not that easy.

The NGP demonstration experiment, even with the improvements suggested above, is far from the "break-even" point of reliably producing more energy than it consumes. Further, the amount of energy it does produce is very small, and the system reliability for long duration operation, depending as it does on the robustness of lithium tantalate crystals against radiation damage, is not at all clear. Like any new technology, it needs to be explored further and is likely to encounter unforeseen problems and produce unforeseen applications.

But in any case, it represents a small, inexpensive, and convenient method of producing a beam of neutrons. This has applications for material studies and for medical cancer treatment and imaging. In the latter context, the NGP group has already demonstrated that it is possible to "tag" the direction an emerging neutron by measuring the direction of the recoiling ^{3}He nucleus that was produced in the same reaction, since the two particles are emitted back-to-back in the system center of mass frame. Thus, if a neutron was scattered by or produced a nuclear reaction in some material, one would know the direction the neutron was traveling before the event occurred. This could have important element-analyzing imaging applications, both in medicine and in areas like homeland security and nuclear weapons safeguards. A space-based variant of the deuteron ionizing setup could also provide the basis for a new type of ion thruster.

Seth Putterman has stated that with this new technology, one could construct a sealed egg-size device, place it in ice water for a while, then hold it in your hand to bring it up to body

temperature, and this would cause it to emit enough neutrons to give you a dangerous radiation dose. That does not sound very useful, but it illustrates the power of this new fusion technology.

1900+14. I. An interpretive study of BeppoSAX and Ulysses observations. *Astrophys. J.* **549,** 1021–1038 (2001).
10. Gaensler, B. M. *et al.* Second-epoch VLA observations of SGR 1806−20. *GRB Circ. Network* **2933** (2005).
11. Corbel, S. & Eikenberry, S. S. The connection between W31, SGR 1806−20, and LBV 1806−20: Distance, extinction, and structure. *Astron. Astrophys.* **419,** 191–201 (2004).
12. Kolpak, M. A., Jackson, J. M., Bania, T. M. & Dickey, J. M. The radial distribution of cold atomic hydrogen in the galaxy. *Astrophys. J.* **578,** 868–876 (2002).
13. Corbel, S. *et al.* The distance of the soft gamma repeater SGR 1806−20. *Astrophys. J.* **478,** 624–630 (1997).
14. Hartmann, D. & Burton, W. B. *Atlas of Galactic Neutral Hydrogen*. Ch. 4, 169 (Cambridge Univ. Press, Cambridge, 1997).
15. Garwood, R. W. & Dickey, J. M. Cold atomic gas in the inner Galaxy. *Astrophys. J.* **338,** 841–861 (1989).
16. Figer, D. F., Najarro, F. & Kudritzki, R. P. The double-lined spectrum of LBV 1806−20. *Astrophys. J.* **610,** L109–L112 (2004).
17. Nakar, E., Gal-Yam, A., Piran, T., Fox, D. B. The distances of short-hard GRBs and the SGR connection. *Astrophys. J.* (submitted); preprint at http://arXiv.org/astro-ph/0502148 (2005).
18. Fuchs, Y. *et al.* ISO observations of the environment of the soft gamma-ray repeater SGR 1806−20. *Astron. Astrophys.* **350,** 891–899 (1999).
19. Gaensler, B. M. *et al.* A stellar wind bubble coincident with the anomalous X-ray pulsar 1E 1048.1-5937: Are magnetars formed from massive progenitors? *Astrophys. J.* **620,** L95–L98 (2005).
20. Pacholczyk, A. G. *Radio Astrophysics. Nonthermal Processes in Galactic and Extragalactic Sources* (Series of Books in Astronomy and Astrophysics, Freeman, San Francisco, 1970).
21. Scott, M. A. & Readhead, A. C. S. The low-frequency structure of powerful radio sources and limits to departures from equipartition. *Mon. Not. R. Astron. Soc.* **180,** 539–550 (1977).
22. Frail, D. A., Waxman, E. & Kulkarni, S. R. A 450-day light curve of the radio afterglow of GRB 970508: Fireball calorimetry. *Astrophys. J.* **537,** 191–204 (2000).
23. Cheng, K. S. & Wang, X. Y. The radio afterglow from the giant flare of SGR 1900+14: The same mechanisms as afterglows from classic gamma-ray bursts? *Astrophys. J.* **593,** L85–L88 (2003).
24. Nakar, E., Piran, T., Sari, R. Giant flares as mini gamma ray bursts. Preprint at http://arXiv.org/astro-ph/0502052 (2005).
25. Wang, X. Y., Wu, X. F., Fan, Y. Z., Dai, Z. G. & Zhang, B. An energetic blast wave from the December 27 giant flare of soft γ-ray repeater 1806−20. *Astrophys. J.* **623**, L29–L32 (2005).
26. Hjellming, R. M. *et al.* Light curves and radio structure of the 1999 September transient event in V4641 Sagittarii (= XTE J1819-254 = SAX J1819.3-2525). *Astrophys. J.* **544,** 977–992 (2000).

Supplementary Information accompanies the paper on **www.nature.com/nature**.

Acknowledgements ATCA is funded by the Commonwealth of Australia for operations as a National Facility managed by CSIRO. We thank K. Newton-McGee and B. Gaensler for scheduling and performing observations with the ATCA. GMRT is run by the National Centre for Radio Astrophysics—Tata Institute of Fundamental Research, India. We thank the GMRT staff and in particular C. H. Ishwara-Chandra and D. V. Lal for help with observations and analysis. The VLA is a facility of the National Science Foundation operated under cooperative agreement by Associated Universities, Inc. NMA is a branch of the National Astronomical Observatory, National Institutes of Natural Sciences, Japan. IRAM is supported by INSU/CNRS (France), MPG (Germany) and IGN (Spain). We thank A. Weiss from IRAM for help with the observations. We gratefully acknowledge discussions with S. Corbel, S. S. Eikenberry and R. Sari. Our work is supported in part by the NSF and NASA.

Competing interests statement The authors declare that they have no competing financial interests.

Correspondence and requests for materials should be addressed to P.B.C. (pbc@astro.caltech.edu).

Observation of nuclear fusion driven by a pyroelectric crystal

B. Naranjo[1], **J.K. Gimzewski**[2,3] **& S. Putterman**[1,3]

[1]*Physics Department,* [2]*Chemistry Department,* [3]*CNSI, University of California Los Angeles, California 90095, USA*

While progress in fusion research continues with magnetic[1] and inertial[2] confinement, alternative approaches—such as Coulomb explosions of deuterium clusters[3] and ultrafast laser–plasma interactions[4]—also provide insight into basic processes and technological applications. However, attempts to produce fusion in a room temperature solid-state setting, including 'cold' fusion[5] and 'bubble' fusion[6], have met with deep scepticism[7]. Here we report that gently heating a pyroelectric crystal in a deuterated atmosphere can generate fusion under desktop conditions. The electrostatic field of the crystal is used to generate and accelerate a deuteron beam (>100 keV and >4 nA), which, upon striking a deuterated target, produces a neutron flux over 400 times the background level. The presence of neutrons from the reaction D + D → ^{3}He (820 keV) + n (2.45 MeV) within the target is confirmed by pulse shape analysis and proton recoil spectroscopy. As further evidence for this fusion reaction, we use a novel time-of-flight technique to demonstrate the delayed coincidence between the outgoing α-particle and the neutron. Although the reported fusion is not useful in the power-producing sense, we anticipate that the system will find application as a simple palm-sized neutron generator.

Because its spontaneous polarization is a function of temperature, heating or cooling a pyroelectric crystal in vacuum causes bound charge to accumulate on faces normal to the polarization. A modest change in temperature can lead to a surprisingly large electrostatic field. For example, heating a lithium tantalate crystal from 240 K to 265 K decreases its spontaneous polarization by $0.0037\,C\,m^{-2}$ (ref. 8). In the absence of spurious discharges, introducing this magnitude of surface charge density into the particular geometry of our experiment (Fig. 1a, b) gives a potential of 100 kV. Attempts to harness this potential have focused on electron acceleration and the accompanying bremsstrahlung radiation[9–12], but using the crystal to produce and accelerate ions has been studied much less. Seeking to drive the D–D fusion reaction (http://www.physics.ucla.edu/~naranjo/ucei/ucei.pdf; http://neer.inel.gov/abstract.asp?ProjectID=126; http://www.binghamton.edu/physics/Brownridge%20Summary.pdf), we set out to develop a method of reliably producing an ion beam of sufficient energy (>80 keV) and current (>1 nA). We demonstrate such a method using a tungsten tip to generate the high field ($>25\,V\,nm^{-1}$) necessary for gas phase field ionization of deuterium.

A cut-away view of our vacuum chamber is shown in Fig. 1c. We mounted a cylindrical (diameter, 3.0 cm; height, 1.0 cm) z-cut $LiTaO_3$ crystal with negative axis facing outward onto a hollow copper block. On the exposed crystal face, we attached a copper disc (diameter, 2.5 cm; height, 0.5 mm), allowing charge to flow to a tungsten probe (shank diameter, 80 μm; tip radius, 100 nm; length, 2.3 mm) (Fig. 1b). The probe geometry was chosen so that the tip field was approximately $25\,V\,nm^{-1}$ when the crystal face was charged to 80 kV.

Our detector arrangement is shown in Fig. 1d. The neutron detector consists of six liquid scintillator (BC-501A and NE213) cells (diameter, 127 mm; height, 137 mm), each optically coupled to a 127-mm Hamamatsu R1250 photomultiplier tube (PMT). One output of each PMT was fed into a logical OR trigger, while the other output was fed into two Acqiris DC270 8-bit (1 gigasample per second) 4-channel digitizers configured as a single 8-channel digitizer. For every trigger, a 650-ns waveform was digitized simultaneously on all channels and written to disk for later analysis.

A typical run is shown in Fig. 2. The chamber's deuterium pressure was held at 0.7 Pa throughout the run. First, the crystal was cooled down to 240 K from room temperature by pouring liquid nitrogen into the cryogenic feedthrough. At time $t = 15$ s, the heater was turned on. At $t = 100$ s, X-ray hits due to free electrons striking the crystal were recorded. At $t = 150$ s, the crystal had reached 80 kV and field ionization was rapidly turning on. At $t = 160$ s and still not above 0 °C, the neutron signal rose above background. Ions striking the mesh and the surrounding aperture created secondary electrons that accelerated back into the crystal, increasing the X-ray signal. At $t = 170$ s, the exponential growth of the ion current had ceased, and the tip was operating in the strong field regime, in which neutral molecules approaching the tip ionize with unity probability. The neutron flux continued to increase along with crystal potential until $t = 220$ s, when we shut off the heater. Then, the crystal lost charge through field ionization faster than the

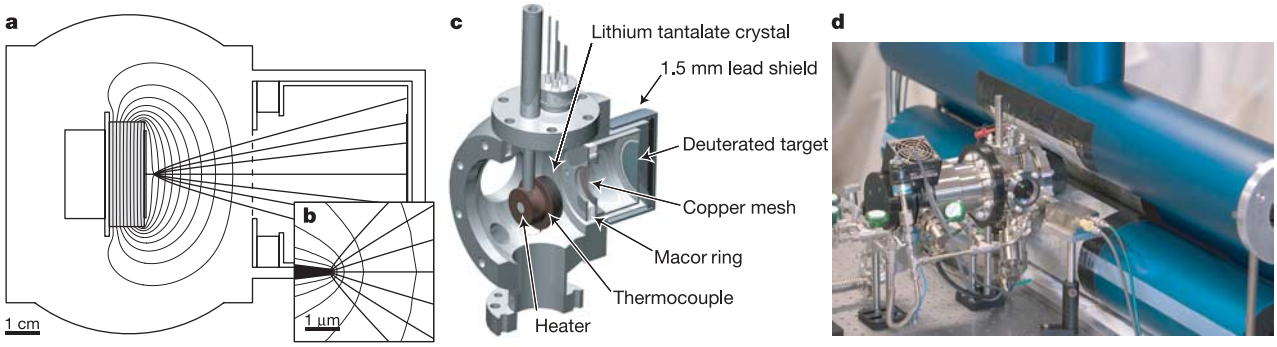

Figure 1 Experiment geometry. **a**, Calculated equipotentials and D^+ trajectories for a crystal charged to 100 kV; calculations were performed using finite-element methods. The grounded copper mesh (85% open area, 19.8-μm wire; vertical dashed line) shields the Faraday cup (right). The cup and target are connected to a Keithley 6485 picoammeter and biased to +40 V to collect secondary electrons and help prevent avalanche discharges. **b**, Same trajectories shown near the tip. Using a shorter tip reduces the beam's angular spread. **c**, Vacuum chamber cut-away view. D_2 pressure was set using a leak valve and monitored with a D_2 compensated Pirani gauge. The target was a molybdenum disc coated with ErD_2. **d**, Arrangement of neutron and X-ray detectors (Amptek XR-100T-CdTe). To better resolve the bremsstrahlung endpoint, a 2.5-cm aluminium filter (not shown) was placed between the X-ray detector and the viewport. The vacuum chamber's thick stainless steel walls and lead sheet shielded the neutron detector from X-rays.

reduced pyroelectric current could replace it, resulting in a steadily decreasing crystal potential. At $t = 393$ s, the crystal spontaneously discharged by sparking, halting the effect.

Pulse shape analysis and proton recoil spectroscopy of neutron detector data collected during the run are shown in Fig. 3. (See Supplementary Methods for details on neutron detector calibration, pulse shape analysis, and a Monte Carlo calculation of detector response and efficiency.) The majority of background triggers, as collected in the first 100 s of the run, have an electron recoil shape (900 counts per second) and are due to cosmic muons and γ-rays, compared with relatively few triggers having a proton recoil shape (33 counts in the first 100 s). Correcting for our 18% 2.45-MeV neutron detection efficiency, the observed peak neutron flux was 800 neutrons per second. We may compare this observed peak

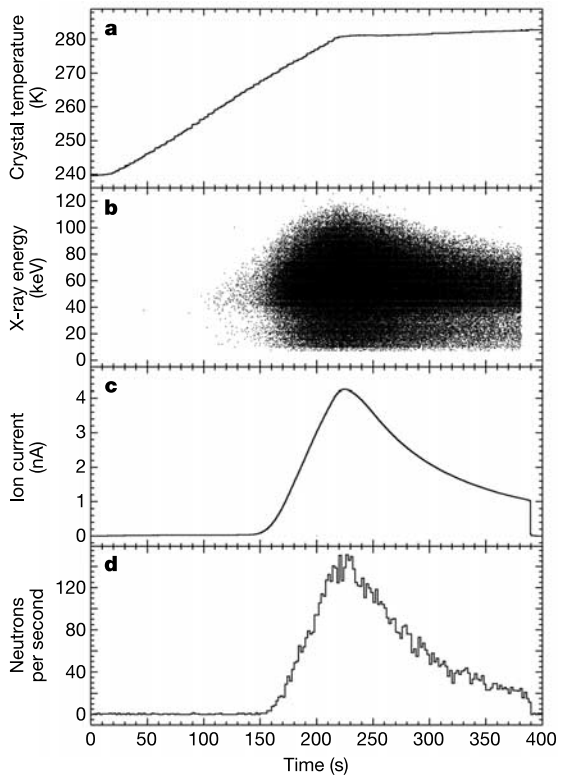

Figure 2 Data from a single run (see also Supplementary Movie 1). **a**, Crystal temperature. The heating rate was 12.4 K min^{-1}, corresponding to a pyroelectric current of 22 nA and a heating power of 2 W. **b**, X-rays detected. **c**, Faraday cup current. **d**, Neutrons detected.

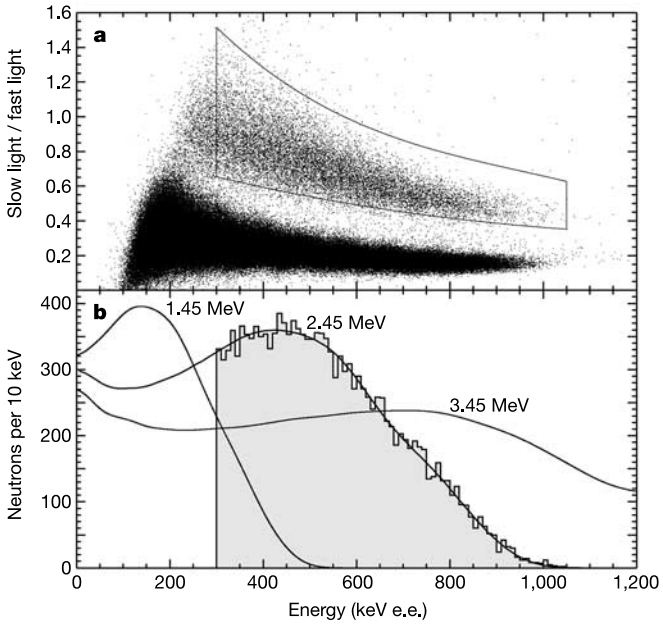

Figure 3 Neutron spectroscopy for the single run. The energy scale, given in electron equivalent (e.e.) energy, was calibrated against Compton edges of a series of γ-ray sources and is proportional to anode charge. **a**, Pulse shape discrimination (PSD) spectrum. Our PSD variable 'slow light/fast light' is the ratio of integrated light in the tail of the PMT signal generated by an event in the liquid scintillator, to the integrated light around the signal's peak. Electron recoils are in the lower branch, and proton recoils, having longer scintillation decay, are in the upper branch. The events enclosed within the upper region are compared against tabulated pulse shapes, rejecting unusual events such as PMT double pulsing. There were a total of 15,300 valid neutrons over the course of the 400-s run. From the distribution of events, we estimate that the number of electron events leaking into the proton branch is negligible compared to the 1% cosmic background. **b**, Proton recoil spectrum. Valid neutron events are shown in histogram format. For comparison, we also show our detector's simulated[20,21] responses to 1.45 MeV, 2.45 MeV and 3.45 MeV centre-of-mass boosted neutrons.

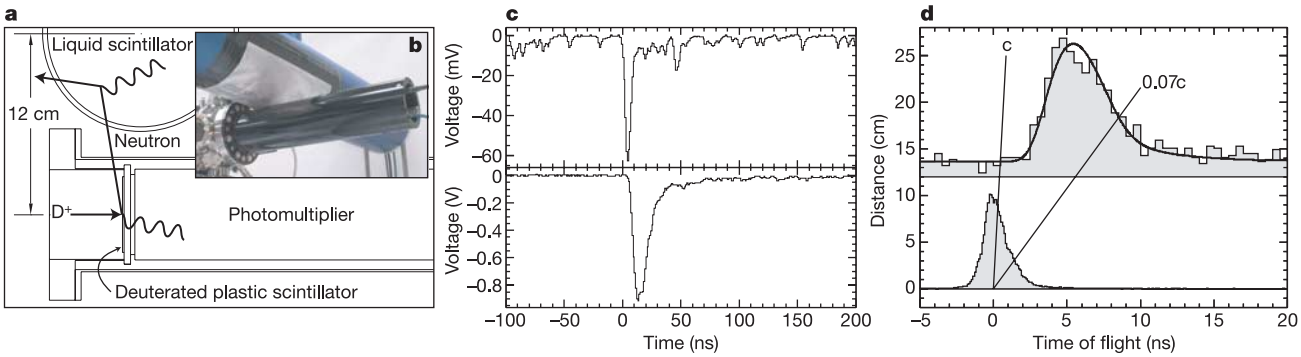

Figure 4 Neutron time-of-flight measurement. **a**, A deuteron is shown striking a thin disk of deuterated plastic scintillator, where it fuses with another deuteron, producing an 820-keV ^{3}He and a 2.45-MeV neutron. The α-particle promptly scintillates in the plastic, recorded by a photomultiplier tube coupled to the glass UHV viewport through a silicone optical pad. The neutron, on the other hand, leaves the vacuum chamber, and is shown detected via proton recoil in the liquid scintillator. **b**, Experiment geometry. **c**, Simultaneously captured PMT traces, demonstrating an α-particle–neutron coincidence. The plastic scintillator trace, shown in the upper panel, has a large α-particle hit at $t = 0$ ns, whereas the smaller hits are incident deuterons that stopped in the plastic but did not fuse. The liquid scintillator trace, shown in the lower panel, has a proton hit at $t = 6$ ns. **d**, Time-of-flight results. The distribution of neutron flight times is shown in the upper histogram. As the neutron emission and detection volumes are finite and relatively closely spaced, we observe a range of flight times. The Monte Carlo flight time distribution, including a constant term to account for background, is shown fitted. The peak in the distribution roughly corresponds with the 5.6 ns it takes a 2.45-MeV neutron moving with a velocity of $0.07c$ (where c is the speed of light) to travel 12 cm. The relative timing offset between the two PMTs was calibrated using back-to-back 511-keV γ-rays from a ^{22}Na source, as shown in the lower histogram.

neutron flux to the neutron flux expected from the ion beam striking the ErD_2 target. At the time of peak neutron flux, the ion current was 4.2 nA and the accelerating potential, inferred from the bremsstrahlung endpoint, was 115 kV. Using tabulated stopping powers[13] and fusion cross-sections[14], we calculate a neutron flux of 900 neutrons s^{-1}. This is a slight overestimate, because part of the ion beam struck outside the target and there was an oxide layer on the target.

In Fig. 4, we present our neutron time-of-flight measurement. Using deuterated plastic scintillator (BC-436) as both a deuterated target, and as a scintillation material, allowed us to pinpoint individual fusion events. The scintillator was mounted inside the chamber against a glass ultrahigh-vacuum (UHV) viewport, through which a Hamamatsu H1949-50 PMT was coupled via a silicone optical pad. The side of the scintillator facing the beam had a 50-nm layer of evaporated aluminium and was connected to the picoammeter. The aluminium prevented the target from charging up, allowed for a reliable beam current measurement, and helped screen out stray light originating from within the chamber. To minimize background hits, yet still collect valid coincidences, we used a reduced deuterium pressure and a reduced heating rate so that the ion current was around 10 pA. Running at this low level permitted prolonged runs. For example, the data shown in Fig. 4d were taken from a single heating cycle lasting over eight hours.

We have shown that small (about centimetre-sized) pyroelectric crystals can produce ion beams (see also Supplementary Fig. 1 and Supplementary Movie 2) of sufficient energy and current to drive nuclear fusion. We anticipate increasing the field ionization current by using a larger tip, or tip array, and by operating at cryogenic temperatures. With these enhancements, and in addition using a tritiated target, we believe that the reported signal could be scaled beyond 10^6 neutrons s^{-1}. Pyroelectric crystals may also have applications in electrostatic fusion devices[15], such as the Farnsworth fusor[16–18], and as microthrusters in miniature spacecraft[19]. □

Received 14 December 2004; accepted 30 March 2005; doi:10.1038/nature03575.

1. Shimomura, Y. & Spears, W. Review of the ITER project. *IEEE Trans. Appl. Supercond.* **14,** 1369–1375 (2004).
2. Miller, G. H., Moses, E. I. & Wuest, C. R. The National Ignition Facility: enabling fusion ignition for the 21st century. *Nucl. Fusion* **44,** S228–S238 (2004).
3. Ditmire, T. *et al.* Nuclear fusion from explosions of femtosecond laser-heated deuterium clusters. *Nature* **398,** 489–492 (1999).
4. Pretzler, G. *et al.* Neutron production by 200 mJ ultrashort laser pulses. *Phys. Rev. E* **58,** 1165–1168 (1998).
5. Taubes, G. *Bad Science: The Short Life and Weird Times of Cold Fusion* (Random House, New York, 1993).
6. Taleyarkhan, R. P. *et al.* Evidence for nuclear emissions during acoustic cavitations. *Science* **295,** 1868–1873 (2002).
7. Saltmarsh, M. J. & Shapira, D. Questions regarding nuclear emissions in cavitation experiments. *Science* **297,** 1603 (2002).
8. Glass, A. M. Dielectric, thermal, and pyroelectric properties of ferroelectric $LiTaO_3$. *Phys. Rev.* **172,** 564–571 (1968).
9. Rosenblum, B., Braunlich, P. & Carrico, J. P. Thermally stimulated field emission from pyroelectric $LiNbO_3$. *Appl. Phys. Lett.* **25,** 17–19 (1974).
10. Riege, H. Electron emission from ferroelectrics—a review. *Nucl. Instrum. Methods A* **340,** 80–89 (1994).
11. Brownridge, J. D., Shafroth, S. M., Trott, D. W., Stoner, B. R. & Hooke, W. M. Observation of multiple nearly monoenergetic electron production by heated pyroelectric crystals in ambient gas. *Appl. Phys. Lett.* **78,** 1158–1159 (2001).
12. Rosenman, G., Shur, D., Krasik, Ya. E. & Dunaevsky, A. Electron emission from ferroelectrics. *J. Appl. Phys.* **88,** 6109–6161 (2000).
13. Ziegler, J. F. The stopping of energetic ions in solids. *Nucl. Instrum. Methods* **168,** 17–24 (1980).
14. Bosch, H. S. & Hale, G. M. Improved formulas for fusion cross-sections and thermal reactivities. *Nucl. Fusion* **32,** 611–631 (1992).
15. Nevins, W. M. Can inertial electrostatic confinement work beyond the ion-ion collisional time scale? *Phys. Plasmas* **2,** 3804–3819 (1995).
16. Farnsworth, P. T. Electric discharge device for producing interactions between nuclei. US Patent No. 3258402 (1966).
17. Farnsworth, P. T. Method and apparatus for producing nuclear-fusion reactions. US Patent No. 3386883 (1968).
18. Hirsch, R. L. Inertial-electrostatic confinement of ionized fusion gases. *J. Appl. Phys.* **38,** 4522–4534 (1967).
19. Mitterauer, J. Micropropulsion for small spacecraft: a new challenge for field effect electric propulsion and microstructured liquid metal ion sources. *Surf. Interface Anal.* **36,** 380–386 (2004).
20. Agostinelli, S. *et al.* GEANT4 — a simulation toolkit. *Nucl. Instrum. Methods A* **506,** 250–303 (2003).
21. Verbinski, V. V. *et al.* Calibration of an organic scintillator for neutron spectrometry. *Nucl. Instrum. Methods* **65,** 8–25 (1968).

Supplementary Information accompanies the paper on **www.nature.com/nature**.

Acknowledgements The neutron detector was built with funds from DARPA. Funding for various stages of this project was provided by the NSF, ONR and DARPA. We thank W. Wright and K. O'Doherty for demonstrations of electron and ion emission from pyroelectrics, respectively; H. Lockart for machine workshop expertise; K. O'Doherty for evaporating the 50-nm film onto the plastic scintillator; R. Cousins for recommending the use of liquid scintillator for detection and pulse-shape identification of neutrons, and for overseeing the design and construction of a prototype detector using waveform digitization; and T. Venhaus, W. Harbin and J. Hoffer of LANL (ESA-TSE group) for supplying the deuterated target. S. P. thanks A. Erbil for bringing the phenomenon of ferroelectric emission to his attention, along with ref. 10.

Competing interests statement The authors declare that they have no competing financial interests.

Correspondence and requests for materials should be addressed to B.N. (naranjo@physics.ucla.edu).